

Interference effects at electron tunneling

N. Angelescu^{*}, M. Bundaru[†], R. Bundaru[‡] and I. Popescu[§]

Abstract

In this article we discuss the interference patterns which appear in the local particle-density and particle-current distributions of two infinite 2-D lattice systems of free fermions which are allowed to communicate via two tunneling junction points. The two fermion reservoirs are initially in different invariant states, and the particle-density and particle-current distributions are calculated in the final stationary state. The dependence of the interference pattern on the interaction details is discussed in several examples.

1 Introduction

The paper is concerned with a simple model of electron tunneling between infinite reservoirs in different equilibrium states. We work in a tight binding approximation, i.e. the electrons live on lattices and the one-particle kinetic energy is given by appropriate lattice Laplace operators. Thereby, the interactions are neglected, so that the Hamilton operators of the isolated reservoirs are bilinear in the electron creation/annihilation operators. At time $t = 0$ a coupling between the reservoirs is switched on, likewise bilinear, which allows direct hopping of the particles between certain finite subsets of sites in different reservoirs. Asymptotically in time, the system approaches a stationary state, in which permanent currents of particles and energy are present. For such models, the approach to stationarity and the structure of the stationary state is well understood at the mathematical level of rigor [1], [2]. The stationary state is a quasi-free state [3], which is completely characterized in terms of the spectral properties of the one-particle Hamilton operators of the free and coupled reservoirs. Explicit formulas for the permanent particle and energy currents between systems are known (the Landauer-Büttiker formulas). However, the state provides more than such global information about the system: it allows obtaining the expectation values of all the local observables.

Our aim here is to perform such a detailed study of the stationary state, by calculating the expectations of various local observables (namely, the local particle density and the particle

^{*}Institute for Physics and Nuclear Engineering "H. Hulubei", P.O.Box MG-6, Bucharest, Romania; e-mail: nangel@theory.nipne.ro

[†]Institute for Physics and Nuclear Engineering "H. Hulubei", P.O.Box MG-6, Bucharest, Romania; e-mail: bundaru@theory.nipne.ro

[‡]Institute for Space Sciences, P.O. Box MG-23, Bucharest, Romania, e-mail: bundaru@spacescience.ro

[§]Institute for Space Sciences, P.O. Box MG-23, Bucharest, Romania

currents) for a particular geometric arrangement and tunneling Hamiltonian. More precisely, we take the reservoirs to be free fermion systems living on regular two-dimensional lattices, with direct tunneling between (one- and/or two-site) finite subsets of the latter. Such choice of the reservoirs is by no means unrealistic, e.g. electrons in the surface states of the close-packed metal surfaces are two-dimensional, nearly free, electron gases. Moreover, the local density of electrons is experimentally accessible by scanning tunneling microscopy, by a technique elaborated in the nineties by Crommie et al [4]. Standing density waves were observed on the Cu(111) surface and their origin explained by the scattering on point impurities located on the surface [4],[5]. Such measurements have since been performed on different materials and defect configurations (see [6] for a recent experiment), and various applications proposed (e.g. [7]). Though our calculations refer to a different physical situation, we hope that they are not only of theoretical interest and that the interference effects exhibited by us can be experimentally observed.

The paper is organized as follows. The precise description of the model and its general properties are done in Section 2. In order to establish notation and for reader's convenience, the approach to, and structure of, the stationary state are presented in Subsection 2.1, following [1], [2]. The main ingredient is the perturbation analysis of the coupled Hamiltonian. As we want to demonstrate the appearance of quantum interference effects in the stationary state, we derive the formulas for the particle density profile (Subsection 2.2) and the local particle currents (Subsection 2.3) in the stationary state. Section 3 is devoted to numerical illustrations. Here, we specify the reservoirs to be two-dimensional free fermion lattice gases, with direct tunneling between (one- and/or two-site) finite subsets of the two square lattices. Subsection 3.1 contains the numerical study of the limit values on the real axis of the Green's function of the two-dimensional lattice Laplacian, which enter the expression of the stationary state. Subsections 3.2, 3.3 are devoted to numerical calculations of the charge- and of the current-density profiles, respectively, for the particular geometry described above. Classically, the total current should be a sum of the currents established through each individual channel when the other are closed. The computations show that this is no longer true in the quantum case. Moreover, the calculated charge-density profiles in the reservoirs exhibit interference fringes, depending on the tunneling constants for every pair of coupled sites. Section 4 is devoted to a discussion of the results.

2 The stationary state

2.1 The model and the approach to stationarity

We consider two lattice free electron gases on $\mathbb{L}_i = \mathbb{Z}^{d_i}$, $i = 1, 2$ (where \mathbb{Z} denotes the integers), coupled via a tunneling junction of finite support. A one-electron wave function is a vector $f \in \mathcal{H} = l^2(\mathbb{L}_1 \cup \mathbb{L}_2) = l^2(\mathbb{L}_1) \oplus l^2(\mathbb{L}_2)$, i.e. $f = \{f_x; x \in \mathbb{L}_1 \cup \mathbb{L}_2\}$, such that $\|f\|^2 := \sum_{x \in \mathbb{L}_1 \cup \mathbb{L}_2} |f_x|^2 < \infty$. Let a_x^* , a_x be the operator of creation, respectively annihilation, of an electron at the site x acting in the anti-symmetric Fock space \mathcal{F} over \mathcal{H} . Also, for $f \in \mathcal{H}$, we denote $a^*(f) = \sum_x f_x a_x^*$ and $a(f) = \sum_x \overline{f_x} a_x$. For a one-particle operator c , given by the

matrix $(c_{x,y})$ ($x, y \in \mathbb{L}_1 \cup \mathbb{L}_2$), its second-quantization, acting in \mathcal{F} , is defined as

$$d\Gamma(c) = \sum_{x,y \in \mathbb{L}_1 \cup \mathbb{L}_2} c_{x,y} a_x^* a_y.$$

Putting the electron mass equal to 1, the one-particle Hamiltonian h^0 corresponding to uncoupled reservoirs, which represents the kinetic energy operator, is given by

$$(h^0 f)_x = \sum_{i=1}^2 (h_i^0 f)_x = -\frac{1}{2} \sum_{i=1}^2 \chi_{\mathbb{L}_i}(x) \sum_{y \in \mathbb{L}_i, |y-x|=1} (f_y - f_x), \quad (2.1)$$

where $\chi_A(x)$ denotes the characteristic function of the set A . The evolution in time (in the Heisenberg picture) of $a^\sharp(f)$ writes as

$$\alpha_t^0(a^\sharp(f)) := e^{itd\Gamma(h^0)} a^\sharp(f) e^{-itd\Gamma(h^0)} = a^\sharp(e^{ih^0 t} f).$$

The generalized eigenfunctions $\phi(k)$ of h^0 are plane waves in each of the two reservoirs, corresponding to given momentum $k \in \mathbb{T}_1 \cup \mathbb{T}_2$, where $\mathbb{T}_i = (-\pi, \pi]^{d_i}$:

$$\text{For } k \in \mathbb{T}_i, \quad \phi(k)_x = \chi_{\mathbb{L}_i}(x) (2\pi)^{-d_i/2} \exp(ikx), \quad (i = 1, 2). \quad (2.2)$$

One has $h^0 \phi(k) = \omega(k) \phi(k)$, where the dispersion law is

$$\omega(k) = \sum_{i=1}^2 \chi_{\mathbb{T}_i}(k) \sum_{\alpha=1}^{d_i} 2 \sin^2 k_\alpha / 2. \quad (2.3)$$

At time $t \leq 0$, the two (uncoupled) reservoirs are supposed to be in different equilibria, defined by inverse temperatures β_i and chemical potentials μ_i , $i = 1, 2$. Let $\langle \cdot \rangle_0$ denote this constrained equilibrium state. The density operator of the state $\langle \cdot \rangle_0$ is

$$(\rho^0)_{x,y} := \langle a_x^* a_y \rangle_0 = \sum_{i=1}^2 \int_{k \in \mathbb{T}_i} dk \phi(k)_x \overline{\phi(k)_y} f_{\beta_i, \mu_i}(\omega(k)) = \sum_{i=1}^2 \int_{k \in \mathbb{T}_i} dk E(k)_{x,y} f_{\beta_i, \mu_i}(\omega(k)), \quad (2.4)$$

where $f_{\beta, \mu}(x) = (1 + e^{\beta(x - \mu)})^{-1}$ is the Fermi function, and where we defined the matrix $E(k)$ by

$$E(k)_{x,y} = \phi(k)_x \overline{\phi(k)_y}, \quad x, y \in \mathbb{L}_1 \cup \mathbb{L}_2. \quad (2.5)$$

The higher order correlations in the state $\langle \cdot \rangle_0$ are calculated in terms of these as:

$$\langle a^*(f_1) \dots a^*(f_m) a(g_1) \dots a(g_n) \rangle_0 = \delta_{m,n} \det M, \quad M_{i,j} = \langle a^*(f_i) a(g_j) \rangle_0 = (g_j, \rho^0 f_i)_\mathcal{H}. \quad (2.6)$$

A state with the latter property is called *quasi-free and gauge-invariant*.

Starting from $t = 0$, a tunneling junction is opened, connecting the finite subsets $S_i \in \mathbb{L}_i$, $i = 1, 2$. The future time evolution is controlled by the perturbed one-particle Hamiltonian

$h = h^0 + v$, where $v = \tau + \tau^*$ with $\tau : l^2(\mathbb{L}_2) \rightarrow l^2(\mathbb{L}_1)$ describing the tunneling of particles from the second to the first reservoir, i.e.

$$(\tau f)_x = \chi_{S_1}(x) \sum_{y \in S_2} t_{x,y} f(y), \quad (2.7)$$

and $\tau^* : l^2(\mathbb{L}_1) \rightarrow l^2(\mathbb{L}_2)$ the tunneling in the opposite direction $(\tau^*)_{x,y} = \overline{t_{y,x}}$. The Heisenberg evolution of $a^\sharp(f)$ for $t > 0$ writes

$$\alpha_t(a^\sharp(f)) := e^{itd\Gamma(h^0+v)} a^\sharp(f) e^{-itd\Gamma(h^0+v)} = a^\sharp(e^{i(h^0+v)t} f).$$

The initial state $\langle \cdot \rangle_0$ is no longer invariant under the new evolution. At time $t > 0$, the state will be the gauge-invariant, quasi-free state $\langle \cdot \rangle_t$ of density operator

$$\rho^t = [e^{-ith^0} e^{ith}]^* \rho^0 e^{-ith^0} e^{ith}, \quad (2.8)$$

here, the factors e^{ith^0} are added for convenience (they commute with ρ^0 , hence do not contribute), as they show that, in far future, the state is given by the Møller operators in the scattering theory for the perturbed evolution. More precisely, we shall use the following result, which is an easy consequence of the general results of [1], [2]:

Proposition 2.1 *In the framework defined above,*

1. *the spectrum of h consists of absolutely continuous spectrum, equal to the spectrum of h^0 , $\sigma_{ac}(h) = \sigma(h^0) = \cup_{i=1,2} [0, 2d_i]$ and of a finite set of eigenvalues, $\sigma_p(h)$, outside $\sigma(h^0)$; thereby, the wave operators*

$$W_\pm := s - \lim_{t \rightarrow \pm\infty} e^{ith} e^{-ith^0} \quad (2.9)$$

exist and establish the unitary equivalence of h^0 with the absolutely continuous part h_{ac} of h : $h_{ac} W_\pm = W_\pm h^0$;

2. *the states $\langle \cdot \rangle_t$ approach in mean, as $t \rightarrow \infty$, a stationary state, i.e. the following limits exist:*

$$\lim_{T \rightarrow +\infty} (1/T) \int_0^T \langle A \rangle_t dt =: \langle A \rangle_{\text{stat}}, \quad (2.10)$$

for all polynomials A in $a^\sharp(f)$;

3. *$\langle \cdot \rangle_{\text{stat}}$ is the gauge-invariant, quasi-free state of density operator*

$$\rho_+ = W_- \rho^0 W_-^* + \sum_{\lambda \in \sigma_p(h)} P_\lambda \rho^0 P_\lambda, \quad (2.11)$$

where P_λ is the projection onto the eigenspace of h corresponding to the eigenvalue λ .

The rest of this section is devoted to deriving computable expressions for the eigenvectors and of the Möller operators.

We start with writing the resolvent operators $r^0(z) = (h^0 - z)^{-1}$ and $r(z) = (h - z)^{-1}$. Clearly, $r^0(z)$ is expressed in terms of the generalized eigenfunctions (2.2) of h^0 as:

$$r^0(z)_{x,y} = \int_{\mathbb{T}_1 \cup \mathbb{T}_2} \frac{E(k)_{x,y}}{\omega(k) - z} dk = \int \frac{P(e)_{x,y}}{e - z} de, \quad (2.12)$$

where $E(k)$ is defined in Eq.(2.5) and $P(e)$ is the integral of $E(k)$ over the energy shell $\Sigma_1(e) \cup \Sigma_2(e)$, with

$$\Sigma_i(e) = \{k \in \mathbb{T}_i; \omega(k) = e\}.$$

Both $E(k)$ and $P(e)$ have block diagonal structure with respect to the reservoirs. In particular, $P(e) = P_1(e) \oplus P_2(e)$ where, denoting $d\sigma_i(k)$ the element of surface area on $\Sigma_i(e)$, we have, explicitly,

$$P(e)_{x,y} = \sum_{i=1}^2 \chi_{\mathbb{L}_i}(x - y) P_i(e)_{x,y} = \sum_{i=1}^2 \chi_{\mathbb{L}_i}(x - y) \int_{\Sigma_i(e)} \frac{d\sigma_i(k)}{|\nabla\omega(k)|} E(k)_{x,y}. \quad (2.13)$$

Thereby, $r^0(z)_{x,y} = \sum_{i=1}^2 \chi_{\mathbb{L}_i}(x - y) g_i(z, y - x)$, where $g_i(z, \cdot) : \mathbb{L}_i \rightarrow \mathbb{C}$ is defined as

$$g_i(z, x) = \int_0^{2d_i} \frac{P_i(e)_{0,x}}{e - z} de. \quad (2.14)$$

To calculate $r(z)$, one has to solve for f the equation $(h^0 - z + v)f = g$. If $z \in \mathbb{C} \setminus \sigma(h^0)$, this is equivalent to $f + r^0(z)vf = r^0(z)g$. Applying v to the latter equation, one gets $(v + vr^0(z)v)f = vr^0(z)g$. Let Π be the projection on the range of v : $\Pi\mathcal{H} = (\ker v)^\perp$. There are two possibilities:

- *The restriction of $v + vr^0(z)v$ to $\Pi\mathcal{H}$ is invertible.* Then, $\Pi f = (v + vr^0(z)v)^{-1}vr^0(z)g$. Once Πf is known, the whole vector f is $f = -r^0(z)v(\Pi f) + r^0(z)g$. For such values of z , $h - z$ has a bounded inverse $r(z)$:

$$r(z) = r^0(z) - r^0(z)Q(z)r^0(z), \quad \text{where } Q(z) = v(v + vr^0(z)v)^{-1}v; \quad (2.15)$$

- *There exists a non-zero vector $\psi \in \Pi\mathcal{H}$, such that $(v + vr^0(z)v)\psi = 0$.* Such values of z are eigenvalues of h with eigenvector $f = -r^0(z)v\psi$. Conversely, if f is an eigenvector of h for the eigenvalue z , then $\Pi f \neq 0$ and $f + r^0(z)vf = 0$. Applying v , it follows that $(v + vr^0(z)v)f = (v + vr^0(z)v)(\Pi f) = 0$. Therefore, $\sigma_p(h)$ equals the set of z with this property and there is a one-to-one correspondence between the eigenspace corresponding to z and $\Pi\mathcal{H} \cap \ker(v + vr^0(z)v)$.

We consider next the Möller operator W_- entering Eq. (2.11). As a prerequisite, we remark that the functions $g_i(\cdot; x)$ defined in Eq. (2.14) are analytic in the complex plane cut along the segment $[0, 2d_i]$ and have finite boundary values, i.e. the limits

$$\lim_{\epsilon \searrow 0} g_i(e \pm i\epsilon, x) =: g_{i,\pm}(e; x) \quad (2.16)$$

exist for all $e \in (0, 2d_i)$ and $x \in \mathbb{L}_i$. As a consequence, and because v has finite range $\Pi\mathcal{H}$, the limit values

$$Q_{\pm}(e) := \lim_{\epsilon \searrow 0} Q(e \pm i\epsilon)$$

exist. Clearly, $Q_{\pm}(e)_{x,y} = 0$ unless $x, y \in S_1 \cup S_2$, so we shall view $Q_{\pm}(e)$ as a matrix indexed by $S_1 \cup S_2$, and denote $Q_{\pm}(e)_{x,y}^{(i,j)}$ its submatrices corresponding to $x \in S_i$ and $y \in S_j$ ($i, j = 1, 2$).

Applying W_- , Eq. (2.9), to a generalized eigenfunction of h^0 , one has:

$$\begin{aligned} [W_- \phi(k)]_x &= \lim_{\epsilon \searrow 0} \int_0^{\infty} \epsilon (\delta_x, e^{-it(h-\omega(k)-i\epsilon)} \phi(k)) dt \\ &= \lim_{\epsilon \searrow 0} (\delta_x, (-i\epsilon r(\omega(k) + i\epsilon) \phi(k))) \\ &= \phi(k)_x - [r_+^0(\omega(k)) Q_+(\omega(k)) \phi(k)]_x \\ &= (\delta_x, [I - r_+^0(\omega(k)) Q_+(\omega(k))] \phi(k)), \end{aligned} \quad (2.17)$$

where we used Eq.(2.15) for $r(z)$ and the obvious relation $(-i\epsilon r^0(\omega(k') + i\epsilon) \phi(k')) = \phi(k')$. Likewise,

$$[W_-^* \phi(k)]_x = (\delta_x, [I - Q_-(\omega(k)) r_-^0(\omega(k))] \phi(k)). \quad (2.18)$$

We shall demonstrate the interference effects on two properties of the stationary state $\langle \rangle_{\text{stat}}$, the permanent currents and the particle density. In the calculations below, *we make the assumption that $t_{x,y}$ (hence, all $h_{x,y}$) are real numbers* (physically, complex $h_{x,y}$ are related to the presence of magnetic fields).

2.2 The permanent currents in the stationary state

Let $N_{\{x\}} = a_x^* a_x = d\Gamma(\chi_x)$ be the particle number operator at the site $x \in \mathbb{L}_1 \cup \mathbb{L}_2$, where χ_x is the projection onto the vector δ_x , i.e. its matrix is $(\chi_x)_{y,z} = \delta_{x,y} \delta_{x,z}$. If the evolution is given by the one-particle Hamiltonian h , the flux of particles from the site x is defined as

$$I_{\{x\}} := -\frac{d}{dt} \alpha_t(d\Gamma(\chi_x))|_{t=0} = -i[d\Gamma(h), d\Gamma(\chi_x)] = d\Gamma([-ih, \chi_x]).$$

In the stationary state, as $\langle \alpha_t(N_{\{x\}}) \rangle_{\text{stat}}$ is independent of time, we have the "continuity equation", saying that the total current flowing from the site x vanishes:

$$J_{\{x\}} := \langle d\Gamma([-ih, \chi_x]) \rangle_{\text{stat}} = 0.$$

The l.h.s. of this equation equals $\sum_{y \in \mathbb{L}_1 \cup \mathbb{L}_2} 2\mathfrak{S} \langle h_{y,x} a_y^* a_x \rangle_{\text{stat}}$. We define the current along the oriented bond $\{x, y\}$ in the stationary state as:

$$j_{x,y} = 2\mathfrak{S} \langle h_{y,x} a_y^* a_x \rangle_{\text{stat}} = 2h_{y,x} \mathfrak{S}(\delta_x, \rho_+ \delta_y). \quad (2.19)$$

Clearly, $j_{x,y} = -j_{y,x}$ and $j_{x,y} = 0$ unless $h_{x,y} \neq 0$, what happens, under our assumptions, only if either $h_{x,y}^0 \neq 0$, implying that x, y are nearest neighbors in one of the two lattices, or $v_{x,y} \neq 0$, implying that $x \in S_1$ and $y \in S_2$, or $x \in S_2$ and $y \in S_1$.

Note that, in view of the fact that all $h_{y,x}$ are real, the eigenvectors of h can be chosen to have real components. It follows that *the point spectrum (i.e. the second term in Eq. (2.11)) does not contribute to $j_{x,y}$* , and Eq. (2.19) writes

$$j_{x,y} = 2h_{x,y} \mathfrak{S}(W_-^* \delta_x, \rho^0 W_-^* \delta_y) = 2h_{x,y} \int_{\mathbb{T}_1 \cup \mathbb{T}_2} \rho^0(k) \mathfrak{S}\{(W_-^* \delta_x, E(k) W_-^* \delta_y)\} dk. \quad (2.20)$$

Let $\Lambda \subset \mathbb{L}_1 \cup \mathbb{L}_2$, and $\chi_\Lambda = \sum_{x \in \Lambda} \chi_x$ be the multiplication by the characteristic function of Λ . Then, $d\Gamma(\chi_\Lambda) = \sum_{x \in \Lambda} a_x^* a_x =: N_\Lambda$ is the number of particles in Λ . The flux of particles out of Λ is

$$I_\Lambda := \sum_{(x,y) \in \partial\Lambda} -ih_{x,y}(a_x^* a_y - a_y^* a_x),$$

where the h -boundary of Λ , $\partial\Lambda$, is the set of ordered pairs (x, y) of sites $x, y \in \mathbb{L}_1 \cup \mathbb{L}_2$ such that $h_{x,y} \neq 0$, $x \in \Lambda$, $y \in \mathbb{L}_1 \cup \mathbb{L}_2 \setminus \Lambda$.

If Λ is finite, then $\langle \alpha_t(N_\Lambda) \rangle_{\text{stat}}$ is finite and independent of t , therefore $J_\Lambda := \langle I_\Lambda \rangle_{\text{stat}} = \sum_{(x,y) \in \partial\Lambda} j_{x,y} = 0$.

If Λ is infinite, then $\langle N_\Lambda \rangle_0$ is infinite, whenever the particle-density is non-zero in the initial state, i.e. $\mu_i > 0$ in Eq. (2.4). The same holds for the evolved states $\langle \cdot \rangle_t$ and their limit $\langle \cdot \rangle_{\text{stat}}$.

We consider below the case $\Lambda = \mathbb{L}_1$, whereby we suppose $\mu_1 > 0$. Then, $N_{\mathbb{L}_1}$ represents the number of particles in the first reservoir, which is a conserved quantity for α_t^0 , i.e. $[N_{\mathbb{L}_1}, d\Gamma(h^0)] = 0$. However, in this case, $\partial\mathbb{L}_1 = \{\{x, y\}; x \in S_1, y \in S_2\}$ is finite, so the stationary current from the first reservoir $J_{\mathbb{L}_1} = \langle I_{\mathbb{L}_1} \rangle_{\text{stat}}$ makes sense and equals

$$J_{\mathbb{L}_1} = \sum_{x \in S_1, y \in S_2} j_{x,y}, \quad (2.21)$$

whereby $h_{x,y} = v_{x,y}$. It is worth mentioning that, for any finite sets Λ_1, Λ_2 , such that $S_1 \subset \Lambda_1 \subset \mathbb{L}_1$ and $S_2 \subset \Lambda_2 \subset \mathbb{L}_2$, the following equalities hold:

$$J_{\mathbb{L}_1 \setminus \Lambda_1} = J_{\mathbb{L}_1 \cup \Lambda_2} = J_{\mathbb{L}_1},$$

showing that the same current traverses any finite contour surrounding S_1 in \mathbb{L}_1 , or surrounding S_2 in \mathbb{L}_2 .

We shall calculate below $j_{x,y}$, Eq.(2.20), for $x \in S_1$, $y \in S_2$, using Eq. (2.18). One has

$$(W_-^* \delta_x, E(k) W_-^* \delta_y) = (\delta_x, [I - r_+^0 Q_+] E(k) [I - Q_- r_-^0] \delta_y),$$

where Q_\pm, r_\pm^0 are calculated at $e = \omega(k)$. Using that both $r_\pm^0(k)$ and $E(k)$ have block-diagonal structure with respect to the reservoirs, one obtains

$$\begin{aligned} j_{x,y} = & 2v_{x,y} \int_{\mathbb{T}_1} dk \rho_1^0 \Im \left[-E_1(k) Q_-^{(1,2)} r_{2,-}^0 + r_{1,+}^0 Q_+^{(1,1)} E_1(k) Q_-^{(1,2)} r_{2,-}^0 \right]_{x,y} \\ & + 2v_{x,y} \int_{\mathbb{T}_2} dk \rho_2^0 \Im \left[-r_{1,+}^0 Q_+^{(1,2)} E_2(k) + r_{1,+}^0 Q_+^{(1,2)} E_2(k) Q_-^{(2,2)} r_{2,-}^0 \right]_{x,y}. \end{aligned} \quad (2.22)$$

Taking advantage of the fact that all factors, but $E_i(k)$, under the integral signs depend solely on $e = \omega(k)$, one can perform the integrals over the energy shells $\Sigma_i(e)$ as in Eq. (2.13):

$$\begin{aligned} j_{x,y} = & 2v_{yx} \int_0^{2d_1} de \rho_1^0(e) \Im \left[-P_1(e) Q_-^{(1,2)}(e) r_{2,-}^0(e) + r_{1,+}^0(e) Q_+^{(1,1)}(e) P_1(e) Q_-^{(1,2)}(e) r_{2,-}^0(e) \right]_{x,y} \\ & + 2v_{yx} \int_0^{2d_2} de \rho_2^0(e) \Im \left[-r_{1,+}^0(e) Q_+^{(1,2)}(e) P_2(e) + r_{1,+}^0(e) Q_+^{(1,2)}(e) P_2(e) Q_-^{(2,2)}(e) r_{2,-}^0(e) \right]_{x,y} \end{aligned} \quad (2.23)$$

The summation over x, y in Eq.(2.23) allows a significant simplification of the expression for the total current:

$$\begin{aligned} J_{\mathbb{L}_1} = & 2\Im \int_0^{2d_1} de \rho_1^0(e) \text{tr}_1 \left(-P_1(e) Q_-^{(1,2)}(e) r_{2,-}^0(e) v + r_{1,+}^0(e) Q_+^{(1,1)}(e) P_1(e) Q_-^{(1,2)}(e) r_{2,-}^0(e) v \right) \\ & + 2\Im \int_0^{2d_2} de \rho_2^0(e) \text{tr}_2 \left(-v r_{1,+}^0(e) Q_+^{(1,2)}(e) P_2(e) + v r_{1,+}^0(e) Q_+^{(1,2)}(e) P_2(e) Q_-^{(2,2)}(e) r_{2,-}^0(e) \right) \\ = & 2\Im \int_0^{2d_1} de \rho_1^0(e) \text{tr}_1 \left(P_1(e) Q_-^{(1,1)}(e) - P_1(e) Q_-^{(1,1)}(e) r_{1,+}^0(e) Q_+^{(1,1)}(e) \right) \\ & + 2\Im \int_0^{2d_2} de \rho_2^0(e) \text{tr}_2 \left(Q_+^{(2,2)}(e) P_2(e) - Q_-^{(2,2)}(e) r_{2,-}^0(e) Q_+^{(2,2)}(e) P_2(e) \right), \end{aligned}$$

where we applied the identity $Q(z)r^0(z)v = vr^0(z)Q(z) = v - Q(z)$ and the cyclic invariance of the trace. Now, $2\Im \text{tr} A = -i \text{tr}(A - A^*)$ and $Q_-^{(i,i)} - Q_+^{(i,i)} = \sum_j Q_+^{(i,j)}(r_{j,+} - r_{j,-}) Q_-^{(j,i)} = \sum_j Q_+^{(i,j)} 2i\pi P_j Q_-^{(j,i)}$, so

$$J_{\mathbb{L}_1} = 2\pi \int_0^{2 \min(d_1, d_2)} de (\rho_1^0(e) - \rho_2^0(e)) \text{tr}_1 \left(P_1(e) Q_-^{(1,2)}(e) P_2(e) Q_+^{(2,1)}(e) \right). \quad (2.24)$$

2.3 The charge-density profile in the stationary state

The charge density at the site $x \in \mathbb{L}_1 \cup \mathbb{L}_2$ in the stationary state is given, according to Eq.(2.11), by:

$$d(x) := \langle a_x^* a_x \rangle_{\text{stat}} = (\delta_x, \rho_+ \delta_x) = d_p(x) + d_{\text{ac}}(x), \quad (2.25)$$

where we separated the contributions of the point and absolutely continuous spectra:

$$\begin{aligned} d_p(x) &= \sum_{\lambda \in \sigma_p(h)} (P_\lambda \delta_x, \rho^0 P_\lambda \delta_x) = \sum_{i=1,2} \int_{k \in \mathbb{T}_i} dk f_{\beta_i, \mu_i}(\omega(k)) \sum_{\lambda \in \sigma_p(h)} |(P_\lambda \phi(k), \delta_x)|^2, \\ d_{\text{ac}}(x) &= (W_-^* \delta_x, \rho^0 W_-^* \delta_x) = \sum_{i=1,2} \int_{k \in \mathbb{T}_i} dk f_{\beta_i, \mu_i}(\omega(k)) |[W_- \phi(k)]_x|^2. \end{aligned} \quad (2.26)$$

Clearly, $\sum_{x \in \mathbb{L}_2} d_p(x) < \infty$, meaning that the number of particles accommodated on the eigenstates of h is finite and located near $S_1 \cup S_2$.

We calculate $d_{\text{ac}}(x)$ for $x \in \mathbb{L}_2$. Remembering Eq.(2.17) and the definition (2.5), we have

$$|[W_- \phi(k)]_x|^2 = (\delta_x, [I - r_+^0(\omega(k))Q_+(\omega(k))]E(k)[I - Q_-(\omega(k))r_-^0(\omega(k))]\delta_x). \quad (2.27)$$

Again, the integration over the energy shell $\omega(k) = e$ can be performed with Eq. (2.13), so, finally,

$$d_{\text{ac}}(x) = \sum_{i=1,2} \int_0^{2d_i} de f_{\beta_i, \mu_i}(e) (\delta_x, [I - r_+^0(e)Q_+(e)]P_i(e)[I - Q_-(e)r_-^0(e)]\delta_x). \quad (2.28)$$

Here, one should take into account the block structure of r^0 and the fact that $P_i(e)_{y,z} = 0$ unless both $y, z \in \mathbb{L}_i$. For instance, if $x \in \mathbb{L}_2$, the term $i = 1$ in Eq.(2.28) simplifies to

$$d^{(1)}(x) = \int_0^{2d_1} de f_{\beta_1, \mu_1}(e) \sum_{s_2, s'_2 \in S_2} g_{2,+}(e; s_2 - x) [Q_+^{(2,1)}(e)P_1(e)Q_-^{(1,2)}(e)]_{s_2, s'_2} g_{2,-}(e; x - s'_2), \quad (2.29)$$

while the term $i = 2$ has a more complicated structure, due to the superposition of the incident and the reflected waves:

$$\begin{aligned} d^{(2)}(x) &= \int_0^{2d_2} de f_{\beta_2, \mu_2}(e) \{ P_2(e)_{x,x} \\ &\quad - \sum_{s_2 \in S_2} \left[g_{2,+}(e; x - s_2) \left(Q_+^{(2,2)}(e)P_2(e) \right)_{s_2, x} + \left(P_2(e)Q_-^{(2,2)}(e) \right)_{x, s_2} g_{2,-}(e; s_2 - x) \right] \\ &\quad + \sum_{s_2, s'_2 \in S_2} g_{2,+}(e; x - s_2) [Q_+^{(2,2)}(e)P_2(e)Q_-^{(2,2)}(e)]_{s_2, s'_2} g_{2,-}(e; s'_2 - x) \}. \end{aligned} \quad (2.30)$$

The following remark is in order. If the dimension $d_2 \geq 2$, the Green function $g_{2,\pm}(e; x) \rightarrow 0$ as $x \rightarrow \infty$. Hence, as $x \rightarrow \infty$ in \mathbb{L}_2 , $d(x)$ approaches the constant $\rho_2 = \int_0^{2d_2} de f_{\beta_2, \mu_2}(e)P_2(e)_{x,x}$, which is the initial equilibrium density of the second reservoir. Indeed, turning on a tunneling junction should not affect the intensive parameters defining the reservoirs, this is one of the reasons why we restrict to dimensions of the lattices larger than 1.

3 Numerical computations

In the computations we particularize to two-dimensional homogeneous reservoirs, i.e. we take $\mathbb{L}_1, \mathbb{L}_2$ both equal to \mathbb{Z}^2 , and h_1^0, h_2^0 both equal to $-(1/2)\Delta$ acting in $l^2(\mathbb{Z}^2)$, see Eq.(2.1). Hence, $\mathbb{T}_1 = \mathbb{T}_2 = \mathbb{T} = (-\pi, \pi)^2$ and the dispersion law of h^0 is $\omega(k_1, k_2) = \sum_{\alpha=1}^2 2 \sin^2(k_\alpha/2)$.

3.1 Evaluation of the Green's function of the 2D Laplacian

We consider here the function $g(z; x) = [(-(1/2)\Delta - z)^{-1}]_{0,x}$. It is defined, for z in the complex plane cut along the real segment $[0, 4]$ and for $x = (x_1, x_2) \in \mathbb{Z}^2$, by the formula (2.12):

$$g(z; x_1, x_2) = (2\pi)^{-2} \int_{\mathbb{T}} dk_1 dk_2 \frac{e^{-i(k_1 x_1 + k_2 x_2)}}{\omega(k_1, k_2) - z}. \quad (3.1)$$

Remark 3.1 *As done in Eq.(2.12), we can integrate first over the energy shells. For $e < 2$, the energy shell $\Sigma(e) = \{k = (k_1, k_2) \in \mathbb{T}; \omega(k) = e\}$ is a closed curve, which can be parametrized by one angle $\theta \in [0, 2\pi)$. Indeed, for all $e \in (0, 2)$ and any θ , there exists one point $k(e, \theta) \in \Sigma(e)$ along that direction. Denoting $K(e, \theta)$ the norm of this k , we have*

$$\begin{cases} k_1(e, \theta) = K(e, \theta) \cos \theta \\ k_2(e, \theta) = K(e, \theta) \sin \theta \end{cases},$$

with $K(e, \theta)$ the unique solution of the equation $\omega(K \cos \theta, K \sin \theta) = e$. The change of variables $(k_1, k_2) \rightarrow (e, \theta)$ is regular from $|k_1| + |k_2| < \pi$ to $(0, 2) \times [0, 2\pi)$ and its Jacobian equals

$$J(e, \theta) = K(e, \theta) \partial_e K(e, \theta). \quad (3.2)$$

Hence, if $e < 2$, and denoting ϕ the polar angle of $x = (x_1, x_2)$, we have

$$P(e)_{0,x} = \frac{1}{(2\pi)^2} \int_0^{2\pi} d\theta J(e, \theta) \exp[-i|x|K(e, \theta) \cos(\phi - \theta)]. \quad (3.3)$$

For $e > 2$, $\Sigma(e)$ consists of four disconnected parts, which can be put together by changes of variables of the form $k'_\alpha = k_\alpha \pm \pi$ into the closed curve corresponding to $\Sigma(4 - e)$ (see Figure 1), which can be parametrized by an angle θ as before.

One can easily see that

$$g(z; x_1, x_2) = g(z; x_2, x_1) = g(z; |x_1|, |x_2|) = (-1)^{1+x_1+x_2} g(4 - z; x_1, x_2) = \overline{g(\bar{z}; x_1, x_2)}. \quad (3.4)$$

Hence, the values of $g(z; x)$ are real for real z outside the segment $[0, 4]$. We plotted in Figure 2, as an example, $\Im g(z; 0, 0)$, which is strictly positive on the upper part of the cut. Also, g is determined by the values $g(z; m, n)$ with $0 \leq m \leq n$ and $\Re z \leq 2$.

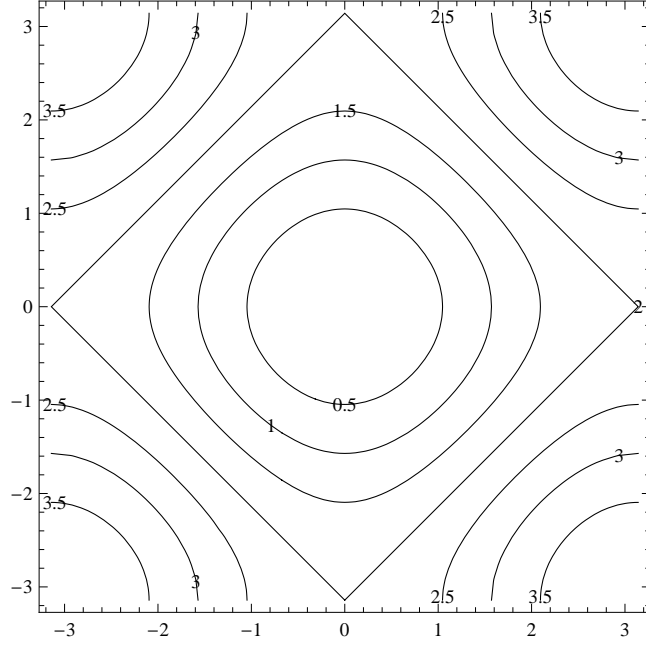


Figure 1: Energy levels $\Sigma(e)$

Using the identity $A^{-1} = i \int_0^\infty e^{-iAt} dt$, if $\Im A < 0$, g can be expressed, for z in the upper complex half-plane, as an integral of a product of two Bessel functions of integer index,

$$g(z; m, n) = i^{m+n+1} \int_0^\infty dt e^{-it(2-z)} J_m(t) J_n(t), \quad (3.5)$$

where we used the representation

$$J_n(t) = \frac{(-i)^n}{2\pi} \int_{-\pi}^{\pi} \exp(-ink + it \cos k) dk.$$

The integral (3.5) is related to a regularized hypergeometric function [8]:

$$g(z; m, n) = \left(-\frac{1}{2}\right)^{m+n+1} \frac{1}{(z-2)^{m+n+1} (m+n)!^2} \cdot {}_4F_3^{reg}(a_1, a_2, a_3, a_4; b_1, b_2, b_3; \frac{4}{(z-2)^2}), \quad (3.6)$$

where

$$a_1 = a_2 = \frac{1+m+n}{2}, \quad a_3 = a_4 = \frac{2+m+n}{2}, \quad b_1 = 1+m, \quad b_2 = 1+n, \quad b_3 = 1+m+n.$$

${}_4F_3^{reg}(\dots; \dots; u)$ is analytic in the complex- u -plane cut along $[1, \infty)$. Note that the limit values $g(e+i0; \dots)$ are expressed in terms of ${}_4F_3^{reg}(\dots; \dots; \frac{4}{(e-2)^2} - i0)$ if $0 < e < 2$.

For m, n not too large (say, $m+n \leq 5$), Eq. (3.6) (including the limit values $g(e+i0; m, n)$ for $0 < e < 4$) can be safely computed using the built-in functions of Mathematica. For larger

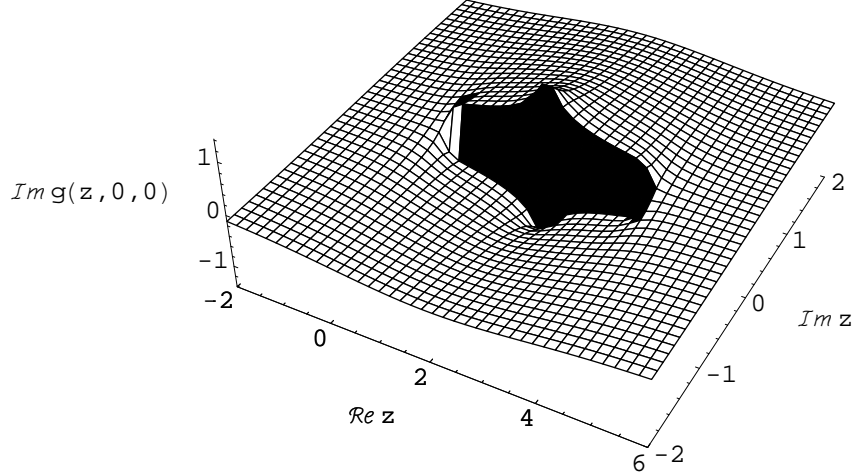


Figure 2: Graph of $\Im g(z; 0, 0)$ in the complex z -plane cut along $[0, 4]$

values of $m + n$, an asymptotic study of g has been performed, based on the steepest descents method [9], [10], the output of which is described below:

For z outside $[0, 4]$, $g(z; x)$ is the Fourier transform of a C^∞ , periodic function of k_1, k_2 , hence it decays faster than any inverse power of the distance $|x|$.

When $z = e + i\epsilon$, $0 < e < 4$, the denominator in Eq. (3.1) develops a singularity in the integration domain when $\epsilon \searrow 0$. As remarked below Eq. (3.4), it is sufficient to consider $e < 2$ and $x = (m, n)$, $m, n \geq 0$. Let $\chi(t)$ be a C^∞ -function, which equals 1 if $|t - e| < a$ and vanishes if $|t - e| > b$, where $0 < a < b < 2 - e$. Then, the asymptotic series of $g(e + i0; x)$ coincides with that of

$$g_\chi(e + i0; x) = (2\pi)^{-2} \int_{\mathbb{T}} dk_1 dk_2 \frac{\chi(2 - e - \cos k_1 - \cos k_2) e^{-i(k_1 m + k_2 n)}}{2 - e - i0 - \cos k_1 - \cos k_2}. \quad (3.7)$$

Therefore, remembering Eq.(3.3),

$$g_\chi(e + i0; x) = \int dt \frac{\chi(t - e)}{t - e - i0} P(t)_{0,x}. \quad (3.8)$$

The phase $\Phi(e, \phi; \theta) = -K(e, \theta) \cos(\phi - \theta)$ in Eq. (3.3) (where $\phi = \arctan(n/m)$ is the direction of $x = (m, n)$) has two stationary points with respect to θ , i.e. the equation $\partial_\theta \Phi(e, \phi; \theta) = 0$ has two solutions $\theta_s(e, \phi) \in [0, \pi/2]$ and $\theta_s(e, \phi) + \pi$, which control the asymptotic behavior. Thereby,

$$\partial_\theta^2 \Phi(e, \phi; \theta)|_{\theta_s} = J(e, \theta_s)^2 \psi(e, \phi) > 0, \quad (3.9)$$

where

$$\psi(e, \phi) = \cos(K_s \cos \theta_s) \sin(K_s \sin \theta_s) \sin \phi + \cos(K_s \sin \theta_s) \sin(K_s \cos \theta_s) \cos \phi, \quad (3.10)$$

Here we denoted, for shortness, $K_s = K(e, \theta_s(e, \phi))$, $\theta_s = \theta_s(e, \phi)$. Likewise, $\partial_\theta^2 \Phi(e, \phi; \theta)|_{\theta_s + \pi} < 0$. Also, $\partial_e \Phi(e, \phi; \theta_s) = -\partial_e K(e, \theta_s) \cos(\phi - \theta_s) < 0$, as $\partial_e K > 0$ and $\phi - \theta_s \in [-\pi/2, \pi/2]$.

A straightforward application of Lemma 7.2.5 of [10] shows that the leading term of the $|x| \rightarrow \infty$ asymptotical series of Eq. (3.8) equals

$$g(e + i0; x) \sim \frac{1}{\sqrt{|x|} \sqrt{2\pi\psi(e, \phi)}} e^{i(|x|K_s \cos(\phi - \theta_s) + \pi/4)}. \quad (3.11)$$

3.2 The density profile

We compute here the density distribution (i.e. the number of band electrons per lattice site) in the second reservoir \mathbb{L}_2 in the stationary state. Thereby, we take the initial equilibria to correspond to zero temperature in both reservoirs, and to chemical potentials μ_1 in \mathbb{L}_1 , and $\mu_2 < \mu_1$ in \mathbb{L}_2 . Hence, the initial (equilibrium) densities in the reservoirs take the values:

$$\rho_{\text{eq}}^{(i)} = \int_0^{\mu_i} P(e)_{0,0} de. \quad (3.12)$$

We choose for exemplification $\mu_1 = 1.4$, $\mu_2 = 0.3$, what corresponds to $\rho_{\text{eq}}^{(1)} = 0.2804$, $\rho_{\text{eq}}^{(2)} = 0.0492$.

Moreover, $S_i = \{s^{i,1}, s^{i,2}\}$, ($i = 1, 2$) consist of two points at distance d_i apart along an axis of \mathbb{L}_i , e.g. $s^{i,1} = (0, 0)$ and $s^{i,2} = (d_i, 0)$. The "contacts" between reservoirs is done by direct tunneling between the two pairs of points, $\{s^{1,j}, s^{2,j}\}$ with tunneling constants t_j , ($j = 1, 2$). Thereby, we fix $d_2 = 20$ and $t_2 = 1$, what proves to be good for a nice visualization of the interference phenomena, while d_1 and t_1 are left as parameters.

Under the assumptions made above, the transmitted and reflected densities in the second reservoir, Eqs. (2.29) and (2.30), acquire the form (for simplicity, we do not exhibit the dependence on d_1 and t_1):

$$d^{(i)}(x) = \int_0^{\mu_i} \delta^{(i)}(e; x) de \quad (i = 1, 2), \quad x \in \mathbb{L}_2, \quad (3.13)$$

where the functions under the integral sign have the following structure:

$i = 1$ (**transmitted**)

$$\delta^{(1)}(e; x) = (V_-(e, x), m_{\text{tr}}(e)V_-(e, x))_{\mathbb{C}^2}, \quad (3.14)$$

where

$$m_{\text{tr}}(e) = Q_+^{(2,1)}(e) \cdot (P(e)|_{S_1 \times S_1}) \cdot Q_-^{(1,2)}(e) > 0, \quad (3.15)$$

with $P(e)|_{S_1 \times S_1}$ denoting the 2×2 matrix $\{P(e)_{s_1, s'_1}, s_1, s'_1 \in S_1\}$ and $V_-(e, x)$ denoting the 2-dimensional vector $\{g_-(e; x - s_2), s_2 \in S_2\}$; the matrices $Q_{\pm}^{(2,1)}(e)_{s_2, s_1}$ were defined

after Eq.(2.16). Clearly, the whole dependence on x is contained in $V_-(e; x)$, whose components are "waves" of the same shape (independent of t_1, d_1) originating at the two points of S_2 . The shape of these waves is given, far from the source, by the levels of the function at the exponent of Eq. (3.11).

The matrix $m_{\text{tr}}(e)$, depending on the details of the interaction v (in particular on d_1, t_1), controls the interference of the two waves. Indeed, Eq. (3.14) describes the squared norm of the linear combination $m_{\text{tr}}(e)^{1/2}V_-(e; x)$.

$i = 2$ (**reflected**)

$$\delta^{(2)}(e; x) = P(e)_{0,0} - 2\Re\left(V_-(e, x), Q_+^{(2,2)}(e)V^{(0)}(e; x)\right)_{\mathbb{C}^2} + (V_-(e, x), m_{\text{ref}}(e)V_-(e, x))_{\mathbb{C}^2}, \quad (3.16)$$

where

$$m_{\text{ref}}(e) = Q_+^{(2,2)}(e) \cdot (P(e)|_{S_2 \times S_2}) \cdot Q_-^{(2,2)}(e) > 0, \quad (3.17)$$

with $V^{(0)}(e; x)$ denoting the 2-dimensional vector $\{P(e)_{x, s_2}, s_2 \in S_2\}$. The first term in Eq. (3.16) is a constant, giving the density per energy and site of "free" electrons of energy e in the initial equilibrium state of the reservoir \mathbb{L}_2 . The last term has the same significance as for Eq. (3.14) with m_{ref} instead of m_{tr} . The middle term is new and gives account of the overlapping between the "waves" originating in S_2 with the free-electron states in \mathbb{L}_2 of energy e .

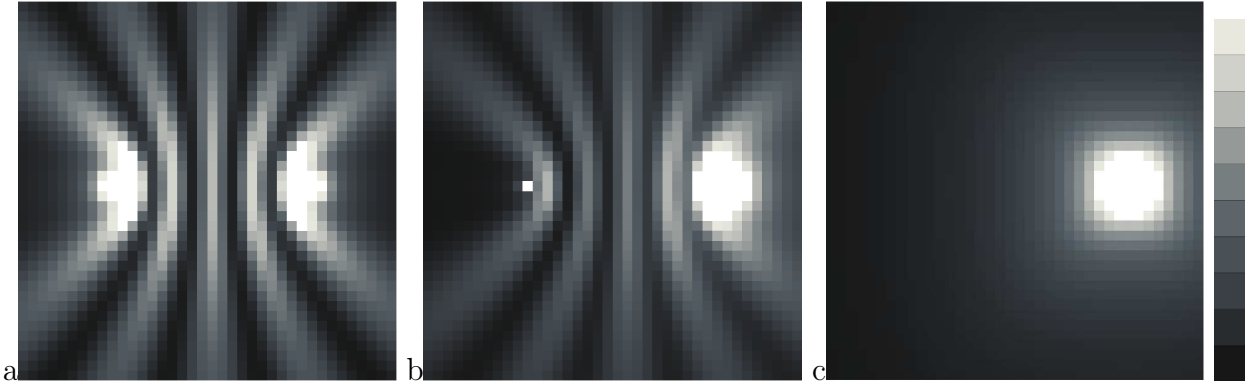


Figure 3: Density plot of $\delta^{(1)}(0.3; x)$ for $t_2 = 1, d_1 = 1$ and: a. $t_1 = 1$; b. $t_1 = 1/2$; c. $t_1 = 0$; Legend values: $k \cdot 10^{-3}, k = 1, \dots, 10$.

We start by exploring the "fixed-energy" density distributions, $\delta^{(1)}$ and $\delta^{(2)}$. In Figures 3 and 4, density plots of $\delta^{(1)}(0.3; x)$ and $\delta^{(2)}(0.3; x)$, respectively, are shown for x in a square of side 40 containing S_2 . Thereby, the cases $t_1 = 1$ (symmetric), $t_1 = 1/2$ (asymmetric) and $t_1 = 0$ (corresponding to one contact) are represented, in order to exemplify the dependence on t_1 . Figure 5 shows the density plot of $\delta^{(1)}(1.4; x)$ in the symmetric case $t_1 = 1$ for a. $d_1 = 1$ and b. $d_1 = 20$; panel c is the plot of $\delta^{(1)}(1.4; x)$ in the case of one contact ($t_1 = 0$).

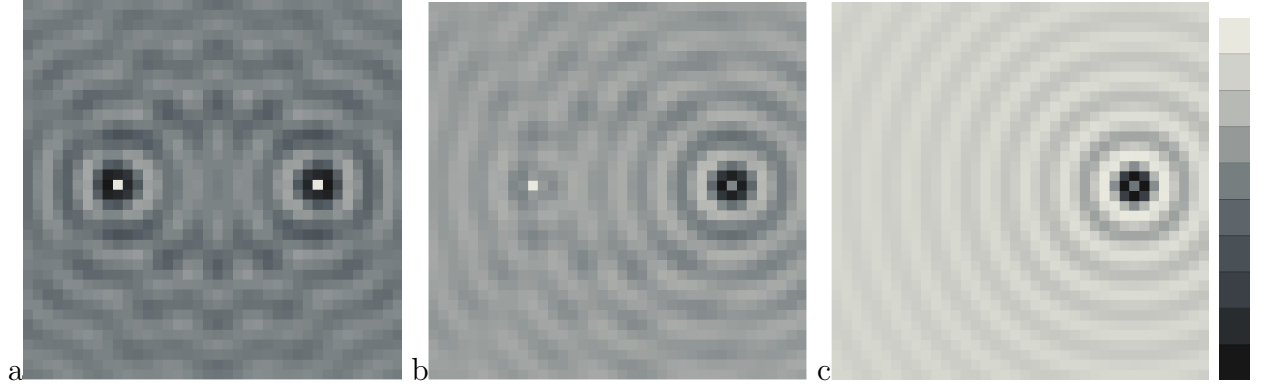


Figure 4: Density plot of $\delta^{(2)}(0.3; x)$ for $t_2 = 1$, $d_1 = 1$ and: a. $t_1 = 1$; b. $t_1 = 1/2$; c. $t_1 = 0$. Legend values: $0.095 + k \cdot 0.012$, $k = 1, \dots, 10$.

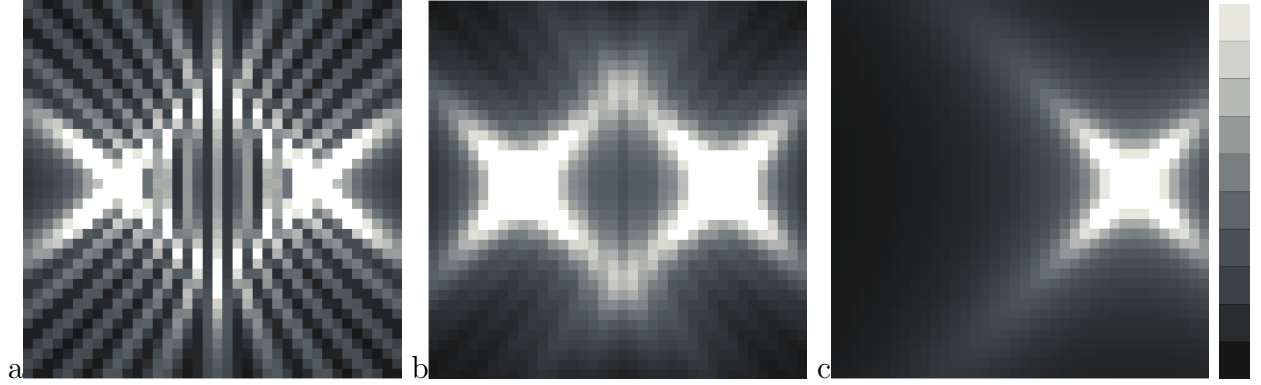


Figure 5: Density plot of $\delta^{(1)}(1.4; x)$ for $t_2 = 1$ and: a. $t_1 = 1$, $d_1 = 1$; b. $t_1 = 1$, $d_1 = 20$; c. $t_1 = 0$. Legend values: $6k \cdot 10^{-4}$, $k = 1, \dots, 10$.

The interference patterns are clearly visible in the symmetric case and $d_1 = 1$ (left panels), but the ones for $\delta^{(1)}$ and for $\delta^{(2)}$ are drastically different. The number of fringes increases with increasing e . In the case of $\delta^{(1)}$, the contrast of the fringes decreases as t_1 decreases, leading, when $t_1 = 0$, to their complete disappearance (panels c in Figures 5 and 4). What concerns $\delta^{(2)}$, "circular" fringes around $s_{2,2}$ survive even at $t_1 = 0$ (Figure 5c).

This can be accounted for using the asymptotic form of $V_-(e, x)$, see Eq. (3.11). Indeed, for $\delta^{(1)}$, the interference of the two components $g_-(e; x - s_2)$, $s_2 \in S_2$ in the linear combination $m_{\text{tr}}(e)^{1/2}V_-(e; x)$ is controlled by the phase difference $|x - s_{2,1}|K_{s,1} \cos(\phi_1 - \theta_{s,1}) - |x - s_{2,2}|K_{s,2} \cos(\phi_2 - \theta_{s,2})$, where we denoted with subscripts 1, 2 the corresponding functions calculated for $s_{2,1}, s_{2,2}$, respectively; taking into account that $K_s \cos(\phi - \theta_s)$ is slowly varying with ϕ (e.g. at $e = 0.3$, it oscillates between 0.784 and 0.795, and its derivative does not exceed 0.022), the above difference is constant (modulo $2k\pi$) on a family of curves similar to hyperbolae with foci $s_{2,1}, s_{2,2}$. The pattern for $\delta^{(2)}$ comes from the second term in Eq. (3.16): as

$V^{(0)}(e; x)$ is a real vector, this term is a sum of cosines, $\cos(\psi_i + |x - s_{2,i}|K_{s,i} \cos(\phi_i - \theta_{s,i}))$, which is constant on curves similar to circles centered at $s_{2,1}, s_{2,2}$. A similar explanation is valid in the situation investigated in [5] and, in fact, the density plots of Figure 4 are quite similar with those reported in [4], [5]. The number of interference fringes depends on e by the monotonicity of the exponent in Eq. (3.11). The fact that the density is higher along diagonals of the lattice, which is striking in Figure 5, is due to the fact that the amplitude $\psi(e, \phi)$ has a minimum (maximum) at $\phi = \pi/4$ (resp 0); at $e = 1.4$, the ratio of $|g_-|^2$ on the diagonal and on the axis (at the same distance from the origin) equals $\psi(1.4, 0)/\psi(1.4, \pi/4) = 2.264$; at $e = 0.3$, this ratio equals only 1.127. This explains, at least for one contact ($t_1 = 0$), why the density is larger on the diagonals and why the effect is better seen at the larger energy (Figures 3c, 4c).

One expects a dependence of $\delta^{(1)}(e; x)$ on the distance d_1 between the two points of S_1 , as the larger d_1 , the less correlated are the electrons incident at two distant contacts. The calculations show that the visibility of the fringes decreases with increasing d_1 (see Figure 5, panel b). However, the interference pattern is conserved even in the limit $d_1 \rightarrow \infty$. Indeed, in this limit $P(e)|_{S_1 \times S_1}$ becomes diagonal, hence, $m_{\text{tr}}(e) = P(e)_{0,0} \lim Q_+^{(2,1)}(e) \cdot \lim Q_-^{(1,2)}(e)$, which is by no means diagonal.

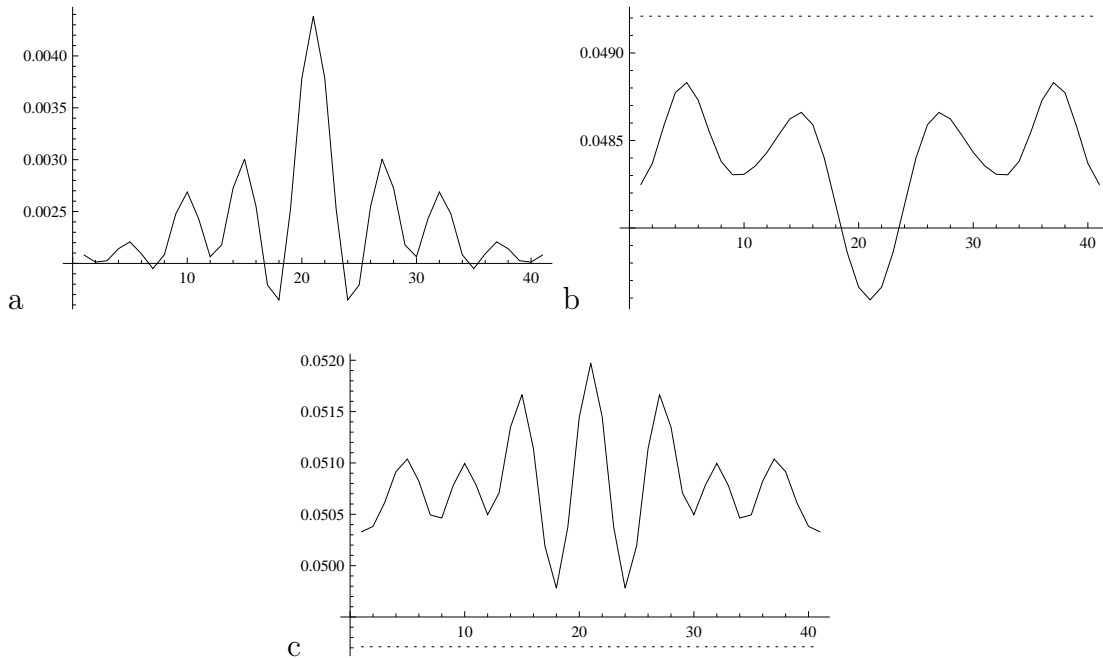


Figure 6: Local densities on the line $x = (i, 19), i = 1, \dots, 40$: a. Transmitted electrons ($\mu_1 = 1.4$); b. Reflected electrons ($\mu_2 = 0.3$); c. The (total) local density in the stationary state. Dashed, the initial equilibrium density is represented.

The density distribution in \mathbb{L}_2 in the stationary state is the sum $d(x) = \int_0^{1.4} \delta^{(1)}(e; x) de + \int_0^{0.3} \delta^{(2)}(e; x) de$. As the position (and number) of the fringes in $\delta^{(i)}(e, x)$ depends on e , we expect the interference pattern of $d(x)$ to have worse visibility. This is confirmed by the computation

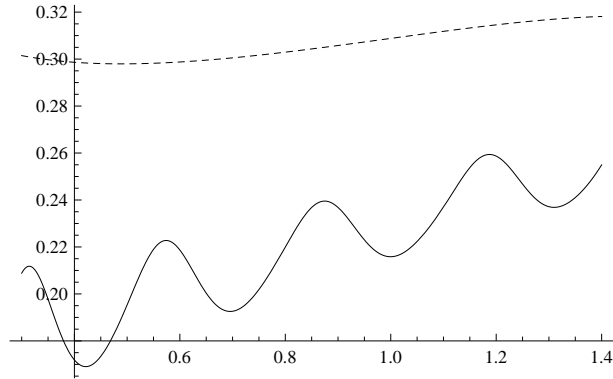


Figure 7: Graph of $j(e)$

of $d(x)$. We fixed, as before, temperature to 0 and $\mu_1 = 1.4$, $\mu_2 = 0.3$. In a density plot of $d(x)$, fringes are indeed hardly visible. Indeed, in the intermediate region where fringes are more pronounced, $d(x)$ is close to the initial equilibrium density of the second reservoir, $\rho_{\text{eq}}^{(2)} = 0.0492$ and has very small oscillations (of order 10^{-3}) around this value. In order to better exhibit the existence of fringes, we plotted the two terms and their sum on the line $x = (i, 19)$, $i = 1, \dots, 40$ in Figure 6.

3.3 The particle current

The total current flowing from reservoir 1 is given by Eq. (2.24). Under the assumptions of the previous subsection, in particular $\beta_1 = \beta_2 = \infty$, $\mu_1 = 1.4$, $\mu_2 = 0.3$, it is easy to see that

$$J_{\mathbb{L}_1} = \int_{0.3}^{1.4} j(e) de; \quad j(e) = 2\pi \text{tr}_2 [m_{\text{tr}}(e)P(e)|_{S_2 \times S_2}], \quad (3.18)$$

with $m_{\text{tr}}(e)$ the same matrix as in Eq. (3.15). We report the calculation for the symmetric case $t_1 = t_2 = 1$ and $d_1 = 1$, $d_2 = 20$: $J_{\mathbb{L}_1} = 0.2416$. It is interesting to exhibit the energy resolution of the current, as well. The plot of $j(e)$, represented in Figure 7, shows oscillations, indicating that tuning the energy may result in higher conductivities. The dotted line in Figure 7 is the plot of $2j_0(e)$, where $j_0(e)$ corresponds to one contact ($t_1 = 0$, $t_2 = 1$, or viceversa). The latter plot, which is what Ohm's law would predict, has no structure and definitely exceeds $j(e)$ over the whole domain.

Interference effects are clearly seen in the distribution of the local currents in a neighborhood of the contacts. We computed, using Eq. (2.20), the local currents in the stationary state in the second reservoir in the same 40×40 square around S_2 , for the same setting and parameter values as before. For $\{x, y\}$ a bond of nearest neighbors in \mathbb{L}_2 , one has, after integration over

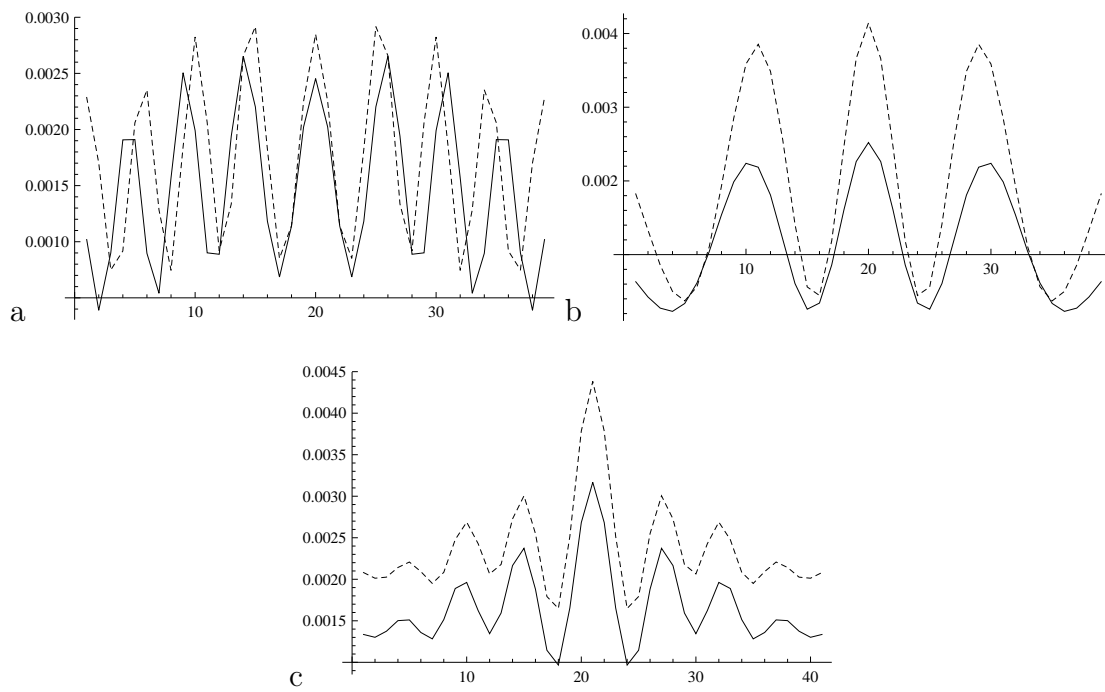


Figure 8: The local "transmitted" current: a. at energy $e = 1.4$; b. at energy $e = 0.3$; c. integrated on the energy range $(0, 1.4)$, across the vertical bonds $\{(i, 19), (i, 20)\}$. Dashed, the local density in points $(i, 19)$ is plotted.

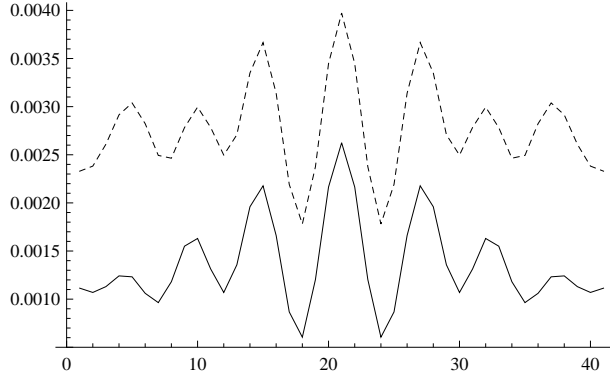


Figure 9: The local currents in the stationary state across the line of bonds $\{(i, 19), (i, 20)\}$, $i = 1, \dots, 40$. Dotted is the local density (shifted downwards with 0.048) at sites $(i, 19)$.

the energy shells,

$$j_{x,y} = \int_0^{0.3} j_{x,y}^{(\text{ref})}(e) de + \int_0^{1.4} j_{x,y}^{(\text{tr})}(e) de,$$

where:

$$\begin{aligned} j_{x,y}^{(\text{tr})}(e) &= -\Im(V_-(e, x), m_{\text{tr}}(e)V_-(e, y))_{\mathbb{C}^2}, \\ j_{x,y}^{(\text{ref})}(e) &= 2\Im\left(V_-(e, x), Q_+^{(2,2)}(e)V^{(0)}(e, y)\right)_{\mathbb{C}^2} - \Im(V_-(e, x), m_{\text{ref}}(e)V_-(e, y))_{\mathbb{C}^2}. \end{aligned} \quad (3.19)$$

Figure 8 is a plot of the local currents of transmitted electrons along nearest-neighbor bonds crossing a horizontal line in the region of fringes: a. of fixed energy $e = 1.4$, i.e. $j_{x,y}^{(\text{tr})}(1.4)$; b. of fixed energy $e = 0.3$, $j_{x,y}^{(\text{tr})}(0.3)$; c. integrated over the whole energy range, i.e. $j_{x,y}^{(\text{tr})} = \int_0^{1.4} j_{x,y}^{(\text{tr})}(e) de$. We took $\{x, y\} = \{(i, 19), (i, 20)\}$, $i = 1, \dots, 40$. We represented also the local density on that line, in order to demonstrate the correlation of the two quantities: currents are larger on bonds starting from high-density sites. The "reflected" local currents $j_{x,y}^{(\text{ref})}$ across the same line show the same kind of correlation with the local density, the major difference being that the currents are negative, i.e. electrons enter the neighborhood of S_2 .

Finally, we plotted in Figure 9 the total (transmitted + reflected) local currents in the stationary state, $j_{x,y}$, on the same line of bonds $\{x, y\} = \{(i, 19), (i, 20)\}$, $i = 1, \dots, 40$, along with a copy of the plot of the local density at x (Figure 6c). As the variation of $j_{x,y}^{(\text{tr})}$ is an order of magnitude larger than that of $j_{x,y}^{(\text{ref})}$, the picture is quite similar to that of $j_{x,y}^{(\text{tr})}$ (Figure 8c), and the same correlation with the total local density is observed.

4 Conclusion

We have performed a detailed study of the stationary state, for the model under consideration, by calculating the expectations of various local observables, namely, the number of particles in

a lattice site and the particle current along a nearest-neighbor bond (in a particular geometric arrangement and tunneling constants). These expectations exhibit a peculiar dependence on the position of the lattice site/bond relative to the two contacts, putting into evidence interference patterns consisting of fringes of high local density, respectively local current. We chose to calculate this space dependence in the less populated of the two systems. Both the density and current profiles are sums of contributions from transmitted and reflected particles (corresponding to one of the systems being unpopulated). The two contributions yield qualitatively different patterns: the fringes of the transmitted particles are similar to hyperbolae with foci in the contacts and they disappear as one of the contacts is suppressed, while the fringes of the reflected particles are similar to circles centered in the contacts and fringes are present even in the case of one contact. We explained this peculiarity, as well as the dependence of the pattern on the various parameters. The space dependence of the sum of the two contributions turns out, in our case, to be dominated by the transmitted particles: hyperbolic fringes of higher density along which particles flow from the contacts to infinity.

New interference effects are to be expected when having, instead of direct tunneling, some finite intermediate quantum system, possibly with a Coulomb repulsion included, in which case the scattering has a resonant structure. For small tunneling constants, resonances come close to the energy levels of the intermediate quantum system, with the effect that only certain energy channels are open. In this case, the fixed-energy calculations performed above become relevant. We propose to follow the subject in another publication.

Acknowledgments

The authors acknowledge financial support from Romanian National Authority for Scientific Research via the programs "Nucleu", contracts NIFIN 3 PN 09 37 and LAPLAS 3 PN 09 39.

References

- [1] W. Aschbacher, V. Jaksic, Y. Pautrat, and C.-A. Pillet 2007 *J.Math.Phys.* **48** 032101
- [2] Angelescu N, Bundaru M and Bundaru R 2008 *Quasi-free Quantum Statistical Models for Tunneling Junctions*, in *Topics in Applied Mathematics and Mathematical Physics* (București: Ed. Acad. Române) pp 11-44
- [3] Bratteli O and Robinson D W 1979 *Operator Algebras and Quantum Statistical Mechanics I* (New York: Springer)
- [4] Crommie M F, Lutz C P and Eigler D M 1993 *Nature* (London) **363** 524
- [5] Heller E J, Crommie M F, Lutz C P and Eigler D M 1994 *Nature* (London) **369** p 464
- [6] Sun G F, Liu Y, Qi Y, Jia J F, Weinert M and Li L 2010 *Nanotechnology* **21** 435401.
- [7] Sentef M, Kampf A P, Hembacher S and Mannhart J 2006 *Phys.Rev. B* **74** 153407.
- [8] H. Bateman (ed.) A. Erdélyi (ed.) 1953 *Higher transcendental functions , 1. The gamma function. The hypergeometric functions. Legendre functions* (New York: McGraw-Hill)
- [9] Erdélyi A 1956 *Asymptotic Expansions* (New York: DoverPubl. Inc.)
- [10] Vainberg B R 1989 *Asymptotic Methods in Equations of Mathematical Physics* (New York: Gordon and Breach)